

Daytime CO₂ urban surface fluxes from airborne measurements, eddy-covariance observations and emissions inventory in Greater London

Article

Accepted Version

Font, A., Grimmond, C. S. B. ORCID: <https://orcid.org/0000-0002-3166-9415>, Kotthaus, S., Morgu, J. -A., Stockdale, C., O'Connor, E., Priestman, M. and Barratt, B. (2015) Daytime CO₂ urban surface fluxes from airborne measurements, eddy-covariance observations and emissions inventory in Greater London. *Environmental Pollution*, 196. pp. 98-106. ISSN 0269-7491 doi: <https://doi.org/10.1016/j.envpol.2014.10.001>
Available at <https://centaur.reading.ac.uk/37905/>

It is advisable to refer to the publisher's version if you intend to cite from the work. See [Guidance on citing](#).

Published version at: <http://dx.doi.org/10.1016/j.envpol.2014.10.001>

To link to this article DOI: <http://dx.doi.org/10.1016/j.envpol.2014.10.001>

Publisher: Elsevier

All outputs in CentAUR are protected by Intellectual Property Rights law, including copyright law. Copyright and IPR is retained by the creators or other copyright holders. Terms and conditions for use of this material are defined in the [End User Agreement](#).

www.reading.ac.uk/centaur

CentAUR

Central Archive at the University of Reading

Reading's research outputs online

1 **Daytime CO₂ urban surface fluxes from airborne measurements, eddy-covariance observations and**
2 **emissions inventory in Greater London**

3 A. Font¹, C. S. B. Grimmond², S. Kotthaus^{2,4}, J.-A. Morgui³, C. Stockdale², E. O'Connor², M. Priestman¹ and B.
4 Barratt¹

5 1 MRC HPA Centre for Environment and Health, King's College London, 150 Stamford Street, SE1 9NH,
6 London, UK

7 2 Department of Meteorology, University of Reading, Earley Gate, PO Box 243, Reading, RG6 6BB, UK

8 3 Institut Català de Ciències del Clima, Dr. Trueta 203, 08005, Barcelona, Spain

9 4 King's College London, Department of Geography, The Strand, WC2R 2LS, London, UK

10 Corresponding author: A. Font (anna.font_font@kcl.ac.uk, telephone: +44 2078484018, fax: +44 2078484045)

11 **Abstract**

12 Airborne measurements within the urban mixing layer (360 m) over Greater London are used to quantify CO₂
13 emissions at the meso-scale. Daytime CO₂ fluxes, calculated by the Integrative Mass Boundary Layer (IMBL)
14 method, ranged from 46 to 104 μmol CO₂ m⁻² s⁻¹ for four days in October 2011. The day-to-day variability of
15 IMBL fluxes is at the same order of magnitude as for surface eddy-covariance fluxes observed in central
16 London. Compared to fluxes derived from emissions inventory, the IMBL method gives both lower (by -37%)
17 and higher (by 19%) estimates. The sources of uncertainty of applying the IMBL method in urban areas are
18 discussed and guidance for future studies is given.

19 **Capsule:** CO₂ airborne-derived fluxes by Boundary Layer Mass balance are an independent measure of meso-
20 scale urban fluxes complementing urban eddy-covariance fluxes and emissions inventory

21 **Key words:** carbon dioxide; urban fluxes; aircraft surveys; eddy covariance; megacity, emissions inventory

22 **1 Introduction**

23 Urban areas are responsible for 70% of greenhouse gas (GHG) emissions despite covering only 2% of the
24 world's surface (IEA 2008). Knowledge of both concentrations and fluxes are needed to understand how urban
25 emissions affect regional carbon exchanges (Duren and Miller 2012).

26 Measurements of urban atmospheric CO₂ concentrations are becoming a common means to study local GHG
27 emissions and urban carbon cycles (Velasco and Roth 2010; Christen 2014). An enhancement of the CO₂
28 concentration of the urban canopy layer (UCL) is consistently observed in cities (e.g. Idso et al. 1998).
29 However, urban CO₂ concentrations can show a high degree of spatial and temporal variability due to different
30 local sources, atmospheric stability and observation locations (e.g. Pataki et al. 2006).

31 Observations of CO₂ fluxes by eddy covariance ($F_{CO_2,EC}$) systems in urban areas have been proven to be a
32 reliable tool to assess carbon exchanges at the neighbourhood or local-scale when conducted above the
33 roughness sublayer (RSL) (e.g. Grimmond et al. 2002; Nemitz et al. 2002; Feigenwinter et al. 2012). Urban
34 areas are a net source of CO₂ (positive fluxes) due to emissions from road traffic, electricity production and local
35 heating with natural gas, oil or coal. Daytime fluxes can be reduced by uptake from vegetation during the
36 growing season, but the nocturnal respiration source remains (Kordowski and Kuttler 2010; Crawford et al.
37 2011; Ward et al. 2013). Where vegetation is scarce in cities, biogenic fluxes contribute little to the total net
38 flux.

39 Diurnal concentrations of CO₂ vary within the boundary layer (BL) as a response to changes in surface
40 emissions, boundary layer growth, entrainment processes and horizontal transport (advection). Taking into
41 account the changing boundary layer (BL) volume and exchanges at its vertical and horizontal ‘boundaries’,
42 meso-scale fluxes (10^2 - 10^4 km²) can be inferred from diurnal changes in CO₂ concentrations observed in the BL,
43 using the Integrative Mass Boundary Layer (IMBL) method (McNaughton and Spriggs 1986; Raupach et al.
44 1992; Denmead et al. 1996; Strong et al. 2011; Christen et al. 2014). The IMBL method has been applied over
45 heterogeneous areas to calculate the mean regional CO₂ surface flux across, for example., the Amazonian basin
46 (Lloyd et al. 2001, 2007) or an agricultural area in Spain (Font et al. 2010), while urban applications include
47 nocturnal CO₂ and CH₄ emissions for Krakow (Poland) (Zimnoch et al. 2010) and turbulent sensible and latent
48 heat fluxes in Sacramento (California, USA) (Cleugh and Grimmond 2001).

49 The aim of this study is to estimate top-down CO₂ emissions at the urban boundary layer (UBL) scale
50 by the IMBL method using airborne observations taken in the UBL of Greater London (GL). This approach
51 assumes that a representative urban CO₂ concentration can be calculated from a transect across a large area of
52 the city or downwind of it. Results of the IMBL method are presented for four case study days, with a sensitivity
53 analysis of the influence of different assumptions being made, and then compared to neighbourhood-scale eddy-
54 covariance measurements and bottom-up emission inventory estimates. Conclusions from this study highlight

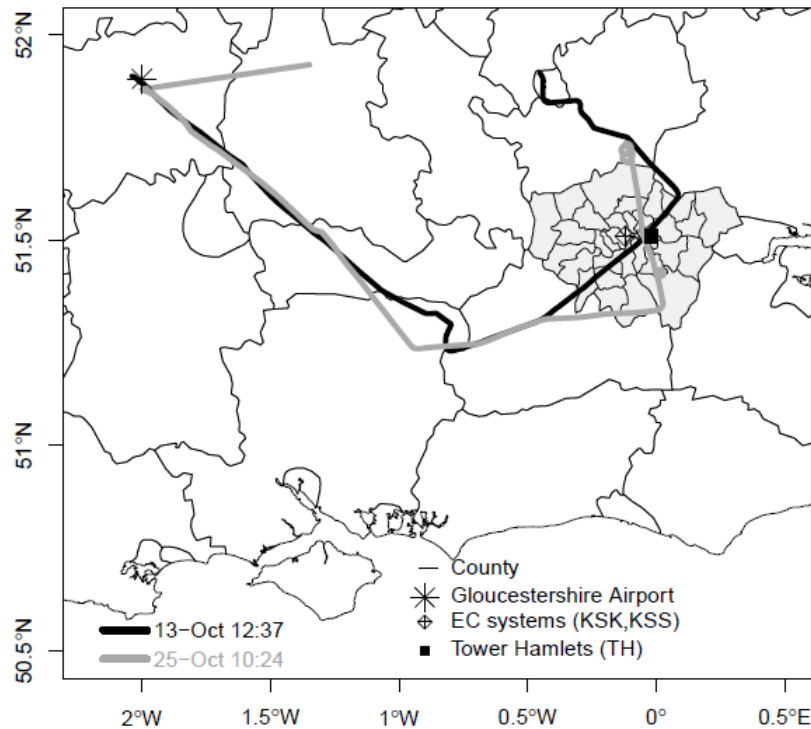
55 the applicability of such airborne observations to quantify CO₂ exchanges of a large city and also highlight the
56 methodological challenges encountered.

57 **2 Methods**

58 **2.1 Instrumentation and survey design**

59 The NERC-ARSF aircraft provided the BL observations between the 12 and 25 October 2011 over
60 South-East England (Table 1). The plane instrumented with an AIMMS-20 Air Data Probe (Aventech Research
61 Inc.) measured temperature, barometric pressure, three components of wind speed and horizontal wind direction,
62 with an instrument accuracy of 0.05°C (temperature), 0.1 kPa (pressure), 0.5 m·s⁻¹ (horizontal wind) and 0.75
63 m·s⁻¹ (vertical wind) (Beswick et al. 2008). Atmospheric CO₂ dry mole fractions were measured with a non-
64 dispersive infrared (NDIR) portable instrument, the CO₂ Airborne Analyzer System AOS Inc., at a frequency of
65 0.5 Hz with a mean precision and accuracy of ±0.23 ppm and ±0.28 ppm, respectively (Font et al. 2008 provide
66 further details). CO₂ concentrations were traceable to the International Standards (WMO-X2007 scale). An
67 isokinetic aerosol intake fed the GRIMM 1.129 Sky-optical particle counter that measured particle mixing ratio
68 in the size range 0.25-32 µm at a frequency of 0.17 Hz.

69 Flights passed over GL at a height of ~360 m above ground level. The air security authority permitted
70 two paths: SW to NE and SSE to NNW (Fig. 1). Flight path directions were chosen from these options to be
71 best aligned with the prevailing wind direction on the respective day. Vertical profiles (up to 2200 m) were
72 undertaken: just after take-off, before landing and on the perimeter of GL (Fig. 1).



73
74 Figure 1. Flight tracks for 13 and 25 October 2011. GL is shaded and symbols indicate site locations of relevant
75 surface stations.
76

77 UCL CO₂ mixing ratios were observed at Tower Hamlets ('TH'; 51.51°N, 0.02°W, 9.2 m agl) (Fig. 1)
78 every 15 minutes from the LiCOR-820 NDIR analyzer. Two-point calibrations are carried out every 15 days
79 with a zero-scrubber (soda lime) and a CO₂ span gas referenced to the International Scale (WMO-X2007).

80 Neighbourhood-scale turbulent surface fluxes ($F_{CO_2,EC}$) were measured at two long-term eddy
81 covariance (EC) sites in central London ('KSS' and 'KSK'; 51.51°N, 0.12°W). Measurement towers (KSS:
82 Aluma T45-H triangular tower; KSK: single tube mast, Clark Masts CSQ T97/HP) had sensors at 49 m (KSS)
83 and 39 m agl (KSK), about 2.2 x and 1.9 x mean building height in the flux source area, respectively. At both
84 KSS and KSK, the EC system consisted of a CSAT3 sonic anemometer (Campbell Scientific) and a
85 Li7500/Li7500A open path infrared gas analyser (LiCOR Biosciences). The data were sampled at 10 Hz and
86 fluxes calculated for 30 minute intervals. Data processing and quality control are described in Kotthaus and
87 Grimmond (2012, 2013a).

88 2.2 Surface fluxes from aircraft observations

89 The Integrative Mass Boundary Layer (IMBL) method, used to calculate spatially and temporally
90 integrated urban CO₂ surface fluxes from the aircraft observations, treats the BL as a box with conserved scalars

91 (Denmead et al. 1996; Guenther et al. 1996). The variation of the mean mixed-layer CO₂ concentration
 92 (expressed in μmolCO₂ m⁻³, [CO₂]) in time ($\partial[CO_2]/\partial t$) at the measurement height (h) within the BL, also
 93 known as storage flux (F_{sig}), is the result of the surface flux ($F_{CO_2,IMBL}$), entrainment (F_e) and advection (F_{adv}):

$$94 \quad h \frac{\partial[CO_2]}{\partial t} = F_{CO_2,IMBL} + F_e + F_{adv} \quad (1)$$

95 F_e is a function of the difference in concentration in the air entrained from above ($[CO_2]_+$), as the BL height (h_L)
 96 changes in time ($\partial h_L/\partial t$), under a vertical velocity (w_+), and within the BL ($[CO_2]$):

$$97 \quad F_e = \left(\frac{\partial h_L}{\partial t} - w_+ \right) ([CO_2]_+ - [CO_2]) \quad (2)$$

98 F_{adv} is the product of the horizontal wind speed U and the spatial CO₂ gradient ($\partial[CO_2]/\partial x$) at height h :

$$99 \quad F_{adv} = -h \left(U \frac{\partial[CO_2]}{\partial x} \right) \quad (3)$$

100 Reorganizing and integrating Eq. (1) in time, the surface flux can be calculated according to:

$$101 \quad F_{CO_2,IMBL} = \langle h \rangle \frac{[CO_2]_2 - [CO_2]_1}{t_2 - t_1} - \left(\frac{h_{L2} - h_{L1}}{t_2 - t_1} - w_+ \right) ([CO_2]_+ - \langle [CO_2] \rangle) + \langle h \rangle \langle U \rangle \left\langle \frac{\Delta[CO_2]}{\Delta x} \right\rangle \quad (4)$$

102 where $\langle \rangle$ denotes temporal and spatial mean values, i.e. $\langle [CO_2] \rangle$ is the mean concentration over the whole spatial
 103 and temporal domain, $[CO_2]_2$ and $[CO_2]_1$ are the concentrations measured at times t_1 and t_2 , respectively, with
 104 the respective mixing heights h_{L1} and h_{L2} , and w_+ and $[CO_2]_+$ refer to h_{L1} and t_1 . $\left\langle \frac{\Delta[CO_2]}{\Delta x} \right\rangle$ is calculated via linear
 105 regression fit to $[CO_2]$ measured at time t_1 with distance when the plane track was perpendicular to the main
 106 wind direction.

107 $[CO_2]$ is calculated from CO₂ mixing ratios, temperature and barometric pressure measurements by the
 108 ideal gas law. Equation 4 is applied in two ways. The first approach assumes that the same temporal changes in
 109 emission rates occur at different locations so that the relative spatial distribution of CO₂ is constant in time. In
 110 this case temporal profiles of $[CO_2]$ measured during the horizontal transects are used. Vertical profiles of CO₂,
 111 particulates, temperature, wind speed and direction at take-off and landing were used to examine the depth of
 112 the BL and its changes in time. The second approach, the ‘‘column model’’ (Jacob, 1999), quantifies differences
 113 in $[CO_2]$ within vertical columns upwind and downwind of the city, both observed along vertical profiles. The
 114 composition of the well-mixed column varies while travelling across the surface due to emissions within the
 115 observational footprint.

116

117 **2.3. Spatial representativeness of the measurements**

118 To determine the likely source area of the BL observations used to calculate $F_{CO_2,IMBL}$, the Lagrangian
119 Particle Dispersion Model FLEXPART (Stohl et al. 2005) was used in backward mode. Using urban roughness
120 values, FLEXPART is driven by the ECMWF meteorological model with $0.2^\circ \times 0.2^\circ$, 91 vertical levels and 3 h
121 resolution. Ten thousand particles were released from a box defined by the aircraft track (longitude, latitude and
122 altitude) for each transect or profile. Each simulation runs back to midnight at the start of the flight day.
123 Analysis at 5 min intervals ($0.05^\circ \times 0.05^\circ$ spatial resolution) allows estimation of the mean residence time of the
124 air in the layer 0 to 300 m agl that potentially influences the CO_2 concentrations.

125 The source area for the local-scale $F_{CO_2,EC}$ is calculated for both flux towers for every 30 min period
126 using the Kormann and Meixner (2001) footprint model. Sources located within a radius of about 1000 m
127 around the KSS site contribute to the turbulent fluxes, with the closest 300 m responsible for 50% of the impact
128 (Kotthaus and Grimmond, 2013b). The source area at KSK is a bit smaller, and individual roughness elements
129 can impact the observations at times when the EC system is within the RSL. The source areas of both sites are
130 dominated by road surfaces and buildings, with only very little contribution from vegetation. Kotthaus and
131 Grimmond (2012) provide further details on micro-scale emissions within the EC source areas.

132 The source area for the concentration observations within the RSL are not formally calculated, but it is
133 known that the integration area is larger for concentrations than flux measurements (Schmid, 1994) and within
134 the RSL individual roughness elements and sources/sinks are more influential than at larger scales. It can be
135 assumed that the local-scale $F_{CO_2,EC}$ footprints are larger than the concentration source areas in the RSL and that
136 flow channelling may elongate the latter along the streets.

137 **2.4 Emissions inventory for Greater London**

138 The Department of Energy and Climate Change reported annual CO_2 emissions by Local Authority
139 (LA) for 2011 (DECC, 2014), segregated into four main categories: industrial and commercial; domestic;
140 transport; and land use change and forestry. The uncertainty of the inventory for the LAs in GL ranges from 1.6
141 to 2.6% (MacCarthy, 2014).

142 To compare $F_{CO_2,IMBL}$ with bottom-up fluxes ($F_{CO_2,inv}$), the annual flux for GL in 2011 was scaled for
143 the footprint area that influenced the airborne measurements as:

$$144 \quad F_{CO_2,inv} = \frac{E_{LA} * R_{t,LA}}{A_{GL} * \sum R_{t,LA}} \quad (5)$$

145 where E_{LA} are annual emissions for each LA ($\text{ktCO}_2 \text{y}^{-1}$), $R_{i,LA}$ is the residence time of air masses in
 146 each LA based on the FLEXPART analysis, and A_{GL} is the area of influence over London. Temporal profiles
 147 accounting for diurnal, day-of-week, and monthly variations of industrial and domestic emissions were
 148 calculated from energy demand statistics. Variations of transport emissions were calculated from temporal
 149 variations of roadside NO_x increments in London. Further details on how temporal profiles were calculated are
 150 given in Appendix A.

151 3 Results

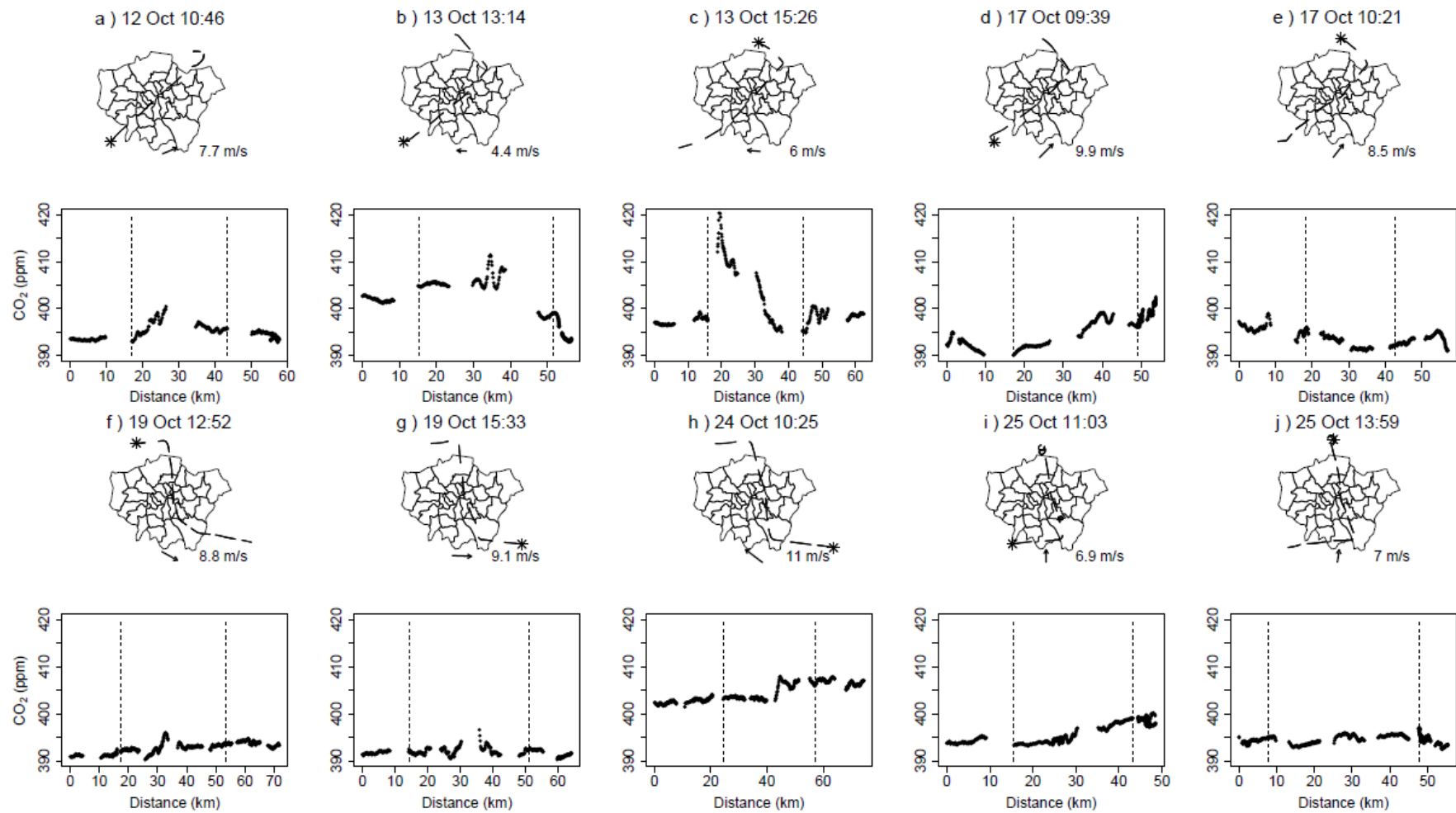
152 3.1 CO_2 mixing ratio observations

153 The spatial variability of CO_2 within and beyond the GL UBL during each flight is shown in Fig. 2. For lower
 154 wind speed conditions ($<8 \text{ m s}^{-1}$ at 360 m), higher CO_2 mixing ratios were measured over central London, with
 155 peaks at 400.5 ppm (12 October 2011), 421.5 ppm (13 October) and 399.1 ppm (25 October), compared to ~ 394 -
 156 398 ppm outside the GL area (Figure 2). With higher wind speed conditions ($>8 \text{ m s}^{-1}$), the differences in
 157 average mixing ratio within and surrounding GL were within the instrument noise (e.g. 17, 24 October) (Table
 158 1). However, for these conditions the maximum measured CO_2 mixing ratio in the mixing layer (407.2 and
 159 409.5 ppm for 17 and 24 October, respectively) was registered downwind of GL at a distance of 29 km (17
 160 October) and 48 km (24 October) from central GL (Fig. SB1).

161

162 Table 1. Mean wind speed (U), mean (± 1 standard deviation σ), maximum and inter-quartile range (IQR) of CO_2 mixing
 163 ratios measured onboard the NERC-ARSF aircraft during the transects across GL (inGL) in October 2011 and
 164 surrounding GL (outGL) below 400 m.

Date, time of flight (UT)	U inGL (m s^{-1})	$\text{CO}_2 \pm 1\sigma$ inGL (ppm)	Max CO_2 inGL (ppm)	IQR CO_2 inGL (ppm)	$\text{CO}_2 \pm 1\sigma$ outGL (ppm)
12 Oct 10:46	7.7	396.1 ± 1.6	400.5	1.9	392.8 ± 1.1
13 Oct 13:14	4.4	404.4 ± 3.3	411.4	1.2	397.5 ± 3.4
13 Oct 15:26	6.0	405.1 ± 7.5	421.8	12.6	398.2 ± 3.3
17 Oct 09:39	9.9	395.1 ± 2.8	399.2	5.1	394.9 ± 3.5
17 Oct 10:21	8.5	392.8 ± 1.4	396.1	2.3	393.5 ± 3.4
19 Oct 12:52	8.8	392.8 ± 0.9	395.9	0.9	392.3 ± 1.6
19 Oct 15:33	9.1	392.1 ± 0.9	396.6	1.1	391.3 ± 0.7
24 Oct 10:25	11.0	404.4 ± 1.6	407.9	2.7	404.4 ± 1.9
25 Oct 11:03	6.9	395.3 ± 1.7	399.1	2.6	394.3 ± 0.9
25 Oct 13:59	7.0	394.9 ± 1.0	397.0	1.3	393.7 ± 0.8



165

166

Figure 2. (Upper) Aircraft flight path over GL starting at location marked by *, with mean wind speed and direction (arrow) measured over GL. Time indicates the start of the transect over GL.

167

(Lower) Measured CO₂ mixing ratios with distance from the indicated start point; vertical dashed lines indicate locations of GL boundary.

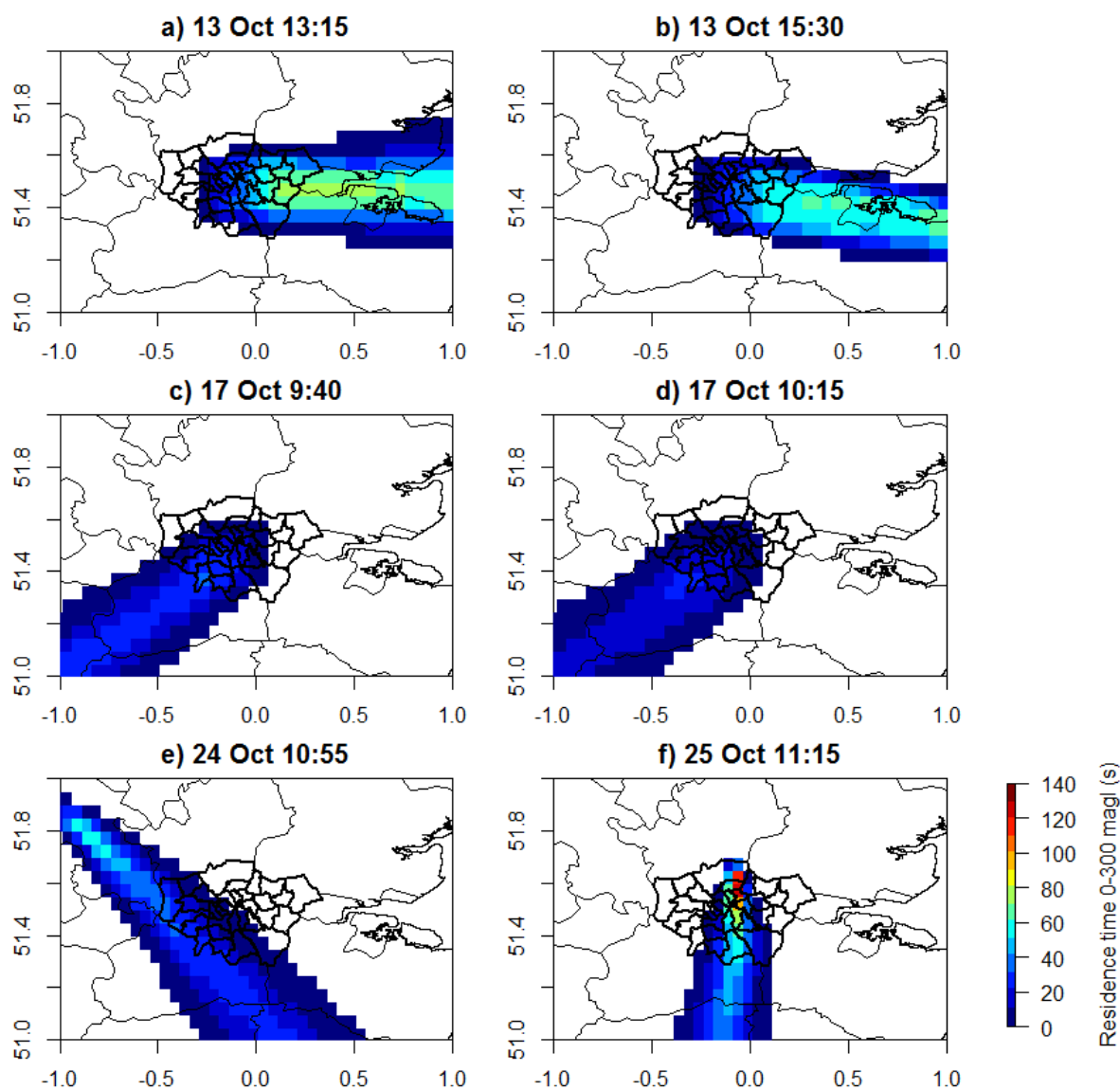
168 3.2 IMBL CO₂ fluxes in Greater London

169 Time and space integrated $F_{CO_2,IMBL}$ for GL were calculated for 13, 17, 24 and 25 October when all
170 terms of the IMBL budget could be identified and quantified. The two IMBL approaches outlined (Section 2.2)
171 were each applied for two of the case study days. First, temporal variations of the mean [CO₂] measured along
172 the transects over GL were used to calculate surface fluxes on 13 and 17 October. Second, downwind profiles
173 were compared to upwind references on 24 and 25 October. Given sufficient data were not available, the IMBL
174 method could not be applied to 12 October (only one transect measured), and 19 October (advection could not be
175 quantified as the flight track was perpendicular to the main wind direction under high wind speeds, see Fig. 2).

176 3.2.1 CO₂ fluxes calculated from horizontal transects

177 The mean wind speed at 360 m over GL on 13 October was 4.4 ± 1.1 m s⁻¹ (morning) and 6.0 ± 1.2 m s⁻¹
178 (afternoon). Visual inspection of vertical profiles showed a well-mixed BL reaching up to a height of 735 m
179 (morning) and at 1180 m (afternoon; Fig. SC1). The flight track flew over the TH site. Mixing ratios measured
180 within the UCL were similar to those measured at 360 m: 405.6 ppm (TH) and 404.4 ppm (aircraft) at 13:15
181 UTC; 407.7 ppm (TH) and 405.1 ppm (aircraft) at 15:30 UTC, suggesting efficient mixing between the ground
182 and flight altitude. The $F_{CO_2,IMBL}$ estimate for this period (13:15 UTC to 15:30 UTC) was $50.7 \mu\text{mol CO}_2 \text{ m}^{-2} \text{ s}^{-1}$.
183 According to the FLEXPART model, the probable source area of the airborne observations covered 71% of GL

184 and included the east (residence time of air 60-80 s) and central boroughs (~20 s) (Fig. 3a,b).



185

186 Figure 3. Air residence time in the layer 0-300 m above ground level (agl) estimated by FLEXPART for flights used in

187

IMBL calculations (Table 2).

188

189

190

191

192

193 Table 2. Values used to calculate the space and time integrated CO₂ urban-regional scale flux ($F_{CO_2,IMBL}$) in GL using the
 194 IMBL budget method. F_{stg} is the storage flux, F_e the entrainment flux and F_{adv} the advection term. $F_{CO_2 inv}$ is the
 195 emissions estimated by DECC (2014).

	13 Oct	17 Oct	24 Oct	25 Oct
t_1 (UTC)	13:15	9:40	10:15	11:05
t_2 (UTC)	15:30	10:15	10:55	11:15
CO ₂ (t_1) (ppm)	404.4	394.8	401.4	394.6
CO ₂ (t_2) (ppm)	405.1	392.8	406.7	398.7
CO ₂₊ (ppm)	391.3	390.0	401.0	394.1
<CO ₂ > (ppm)	404.7	393.7	401.4	394.6
h_1 (m)	735	400	410	450
h_2 (m)	1180	1130	480	450
w_+ (mm s ⁻¹)	-2.5	-0.18	-2.2	-5.6
<U> (m s ⁻¹)	4.5	9.9	---	---
$\langle \frac{\Delta[CO_2]}{\Delta x} \rangle$ ($\mu\text{mol CO}_2 \text{ m}^{-2}$)	---	$1.1 \cdot 10^{-2}$	---	---
F_{stg} ($\mu\text{mol CO}_2 \text{ m}^{-2} \text{ s}^{-1}$)	0.3	-21.5	25.7	103.3
F_e ($\mu\text{mol CO}_2 \text{ m}^{-2} \text{ s}^{-1}$)	-50.4	-29.5	-11.6	-1.1
F_{adv} ($\mu\text{mol CO}_2 \text{ m}^{-2} \text{ s}^{-1}$)	---	-37.9	---	---
$F_{CO_2,IMBL}$ ($\mu\text{mol CO}_2 \text{ m}^{-2} \text{ s}^{-1}$)	50.7	46.0	37.2	104.3
$F_{CO_2 inv}$ ($\mu\text{mol CO}_2 \text{ m}^{-2} \text{ s}^{-1}$)	42.7	54.5	60.4	145.1
Area GL covered (%)	71	56	50	30

196
 197 Vertical profiles of temperature in the morning of 17 October indicated inversion layers at 390-436 m
 198 and at 460-500 m (Fig. SC2). This translated into a decrease in the CO₂ mixing ratios with altitude: ~401.5 (TH)
 199 and 395.1 ppm (aircraft). Later that day (11:56 UTC) the UBL attained 1130 m so that CO₂ mixing ratios were
 200 observed to be vertically homogenous below the cruise altitude (392.3 ppm at TH, 392.8 ppm at 360 m). Given
 201 the strong wind speed conditions and the flight track parallel to the main wind flow (Fig. 2), the 17 October was
 202 the only case study day when it was possible to calculate $\langle \frac{\Delta[CO_2]}{\Delta x} \rangle$ from Eq. 3 and F_{adv} (Table 2). F_e was negative
 203 as air masses with less concentration than below were entrained and CO₂ was lost by advection. F_{stg} was
 204 negative due to the expansion of the UBL in time. At $46.0 \mu\text{mol CO}_2 \text{ m}^{-2} \text{ s}^{-1}$ $F_{CO_2,IMBL}$ was in the same order of
 205 magnitude as on 13 October. The source area coincides with large parts of GL (65%), encompassing areas in
 206 central and south-west GL (Fig. 3c,d).

207 3.2.2 CO₂ fluxes calculated from upwind and downwind vertical profiles

208 On 24 and 25 October, strong wind speed conditions and the prevalent wind direction allowed
 209 Lagrangian observations of two vertical profiles, one upwind and the other downwind of GL. An increase of the
 210 CO₂ mixing ratio was observed in the downwind profiles compared to those upwind by 4-5 ppm (Fig. SC3,
 211 SC4).

212 Strong winds from the SE (12 m s^{-1}) were measured over GL at 360 m altitude on 24 October. Both the
213 vertical profiles upwind and downwind of GL revealed large CO_2 mixing ratios of >400 ppm at low altitudes
214 (<500 m), with a sharp decrease to lower values (391 ppm) above a capping inversion. The strong inversion
215 conditions on that day might have resulted in a residual layer with large CO_2 mixing ratios. The height of the
216 lowest inversion layer increased from 410 m (upwind) to 460 m (downwind). The derived flux $F_{\text{CO}_2, \text{IMBL}}$ was
217 similar in range to 13 and 17 October ($37.2 \mu\text{mol CO}_2 \text{ m}^{-2} \text{ s}^{-1}$ between 10:10 and 10:57). The probable source
218 area covered is 60% of GL with an emphasis of western parts (Fig. 3e).

219 On 25 October wind speeds were 7 m s^{-1} with a prevailing flow from the south. Given no strong
220 inversion was present, absolute mixing ratios were lower than on the preceding day and remained below
221 400 ppm. There was an increase of ~ 4 ppm from the upwind to the downwind locations but the very low
222 entrainment flux as no changes in the UBL height were considered (Fig. SC4), translated to a very high $F_{\text{CO}_2, \text{IMBL}}$
223 estimate of $104.3 \mu\text{mol CO}_2 \text{ m}^{-2} \text{ s}^{-1}$ between 11:05 and 11:15. The source area was estimated to be smaller than
224 on the other case study days, covering only 30% of the GL including areas in north, central and south London
225 (Fig. 3f).

226 3.2.3 Sensitivity analysis of $F_{\text{CO}_2, \text{IMBL}}$

227 Sensitivity analyses allow quantification of the impact of values used within $F_{\text{CO}_2, \text{IMBL}}$ calculations.
228 Assuming uniform temporal changes, the spatial variability of $[\text{CO}_2]$ at 360 m across GL relates to the
229 differences in emissions at different locations (Table 1, Fig. 2). On one case study day (13 October), the
230 standard deviation of $[\text{CO}_2]$ measured along the transects were as high as 7.5 ppm and the inter-quartile range
231 (IQR) reached up to 12.6 ppm. This spatial variation in mixing ratio suggests that there may have been a series
232 of internal BL across GL and horizontal mixing did not have enough time to create a representative spatial
233 pattern at the flight height (360 m). Standard deviation and IQR were generally lower for the other case studies
234 (Table 1). As the $[\text{CO}_2]$ values used to calculate $F_{\text{CO}_2, \text{IMBL}}$ are critical, the variation of CO_2 along the transect was
235 used to assess the accuracy of the flux calculated. Other variables that are used for the $F_{\text{CO}_2, \text{IMBL}}$ calculations are:
236 mixing layer height, vertical velocity at the top of the UBL and temporal and spatial homogeneity of the
237 background concentration. The impact of potential uncertainties in these components on the total uncertainty of
238 the integrated boundary layer CO_2 flux are assessed from the horizontal transects over the urban area and both
239 upwind and downwind vertical profiles (Table 3).

240

241 Table 3. Sensitivity of $F_{CO_2,IMBL}$ to data used in the analysis. $mean [CO_2]_a$: average mixing ratio from aircraft observations;
 242 $mean [CO_2]_{a+s}$ average mixing ratio from aircraft and urban canopy layer; $5^{th} p [CO_2]_a$: 5th percentile mixing ratio
 243 from aircraft observations; $95^{th} p [CO_2]_a$ 95th 95th percentile mixing ratio from aircraft observations; $h+50m$ and
 244 $h+100m$ refer to mixing layer height determined from visual inspection from profiles carried outside GL plus 50 and
 245 100 m, respectively; $no w_+$ and $2 \cdot w_+$ refer to zero and double vertical wind speed above the mixing layer,
 246 respectively; F_{adv,t_2} refers to advection term calculated using the spatial gradient at t_2 . The median value and range
 247 (maximum-minimum) for the fluxes for each day are also given.

Method	$F_{CO_2,IMBL}(\mu molCO_2 m^{-2} s^{-1})$			
	13 Oct	17 Oct	24 Oct	25 Oct
$mean [CO_2]_a$	50.7	46.0	37.2	104.3
$mean \{[CO_2]_{a+} [CO_2]_s\}$	49.2	34.9	---	---
$5^{th} p [CO_2]_a$	30.7	41.6	34.5	133.8
$95^{th} p [CO_2]_a$	82.3	70.7	33.6	89.0
$h + 50 m$	56.1	48.0	42.8	136.8
$h + 100 m$	61.4	50.0	51.4	171.7
$no w_+$	47.5	46.0	33.6	100.8
$2 \cdot w_+$	54.0	46.0	45.2	146.3
F_{adv,t_2}	---	24.7	---	---
Median F_{CO_2}	52.4	46.0	37.2	133.8
Range F_{CO_2}	51.6	46.0	17.8	82.7

248
 249 To evaluate the impact of horizontal spatial variability of $[CO_2]$ on $F_{CO_2,IMBL}$, the mean values are
 250 replaced with the 5th and 95th percentile of $[CO_2]$, respectively (Table 3). The resulting $F_{CO_2,IMBL}$ varied from
 251 30.7 to 82.3 $\mu molCO_2 m^{-2} s^{-1}$ (13 October) and from 41.6 to 73.0 $\mu molCO_2 m^{-2} s^{-1}$ (17 October). Use of these
 252 extreme $[CO_2]$ values generates a difference of up to 60% in the flux relative to that calculated from the mean
 253 $[CO_2]$.

254 Aircraft measurements at 360 m might not capture the vertical gradient within the whole UBL. CO_2
 255 mixing ratios measured at TH were used to calculate $F_{CO_2,IMBL}$. $F_{CO_2,IMBL}$ decreased from 50.7 (aircraft) to 49.2
 256 $\mu mol CO_2 m^{-2} s^{-1}$ (aircraft+TH) (13 October), and from 46.0 (aircraft) to 34.9 $\mu mol CO_2 m^{-2} s^{-1}$ (aircraft+TH)
 257 (17 October). Heterogeneity in the vertical domain in the UBL represent a change of 3% (13 October) and 25%
 258 (17 October) from $F_{CO_2,IMBL}$ calculated from the mean $[CO_2]$ in the transects.

259 Similarly, to evaluate the impact of the variability of the $[CO_2]$ in the air column for fluxes calculated
 260 from upwind-downwind profiles, the 5th and 95th percentile values of $[CO_2]$ were used. This resulted in an
 261 increase of $F_{CO_2,IMBL}$ to 33.6 $\mu mol CO_2 m^{-2} s^{-1}$ (using the 5th percentile) and to 34.5 $\mu mol CO_2 m^{-2} s^{-1}$ (95th

262 percentile) on 24 October (increase of ~56%). Whereas on 25 October, using the 5th percentile values of [CO₂]
263 fluxes were 89.0 (decrease of 15%) but the 95th percentile resulted in a higher flux of 133.8 μmol CO₂ m⁻² s⁻¹
264 (increment of 28%). Unfortunately, UCL measurements of CO₂ directly below the vertical profiles were not
265 available. However, the comparison of observations within the UCL with aircraft measurements near TH reveals
266 that CO₂ mixing ratios hardly differed: 400 ppm (TH) and 400-402 (aircraft) on 24 October; 396 ppm (TH) and
267 395 ppm (aircraft) on 25 October. This indicates the CO₂ field below the aircraft was well-mixed, so little
268 variation in $F_{CO_2,IMBL}$ would be expected.

269 The advection term can be an important part of the CO₂ budget. Without transects parallel to the main
270 wind direction (13 October) the spatial variability of CO₂ and therefore advection could not be quantified.
271 Assuming that the spatial gradient measured on 17 October was the same as on 13 October, the estimated
272 advection flux is 1.6 μmol CO₂ m⁻² s⁻¹ or a probable error in $F_{CO_2,IMBL}$ of 4% from omitting advection for that
273 day. However, for days with higher wind speeds (e.g. 17 October), omission of the advection term could
274 represent an error of ~80%.

275 The uniformity in time of the spatial gradient might also be a source of uncertainty for the advection
276 term. If the spatial gradient on 17 October was calculated at time t_2 , the $F_{CO_2,IMBL}$ would decrease by ~50%
277 calculated to 24.7 μmolCO₂ m⁻² s⁻¹.

278 BL heights were estimated from profiles outside of London. Spanton and Williams (1988) found that
279 the BL height in London could be 50-100 m higher than at a rural site. This in accordance with the difference
280 found between the BL heights from the ceilometer at central London and from vertical profiles for the 24
281 October (day when backscattered data from ceilometer were clearly detected, Appendix C). $F_{CO_2,IMBL}$ calculated
282 with a BL 100 m higher resulted in larger fluxes by 21% (13 October), 5% (17 October), 38% (24 October) and
283 68% (25 October) compared to previous calculations. This test underlines the critical impact of the mixing
284 height on CO₂ exchanges within the UBL.

285 As the small vertical velocity at the BL height is difficult to measure reliably from aircraft (Stull, 1988;
286 Beswick et al. 2008), the sensitivity of $F_{CO_2,IMBL}$ to errors in w_+ were examined assuming $w_+=0$ and doubling the
287 observed w_+ . Using the former ($w_+=0$) $F_{CO_2,IMBL}$ decreases by 6.4% (13 October), 0.1% (17 October), 10% (24
288 October), 3.3% (25 October). Whereas the latter (doubling) increases $F_{CO_2,IMBL}$ by 6.4% (13 October), 21% (24
289 October) and 40% (25 October).

290 The entrainment flux is also be affected by the determination of $[CO_2]_+$. In this study we have used the
291 concentration just above the mixing layer in vertical profiles undertaken outside GL, assuming that this
292 concentration is spatially homogenous for the area between the city and the location of the vertical profile, and
293 also for the integration time used in the IMBL calculations. Ideally, measurements of the entrainment
294 concentration above the UBL would be used.

295 The range of $F_{CO_2,IMBL}$ was lower (50-80% the median value) for fluxes calculated from upwind-
296 downwind profiles compared to the range of fluxes from horizontal transects over the city (100%). However,
297 this is as expected as single pairs of vertical profiles sample a limited area of the urban region (30-50%)
298 compared to the area covered by horizontal transects (60-70%).

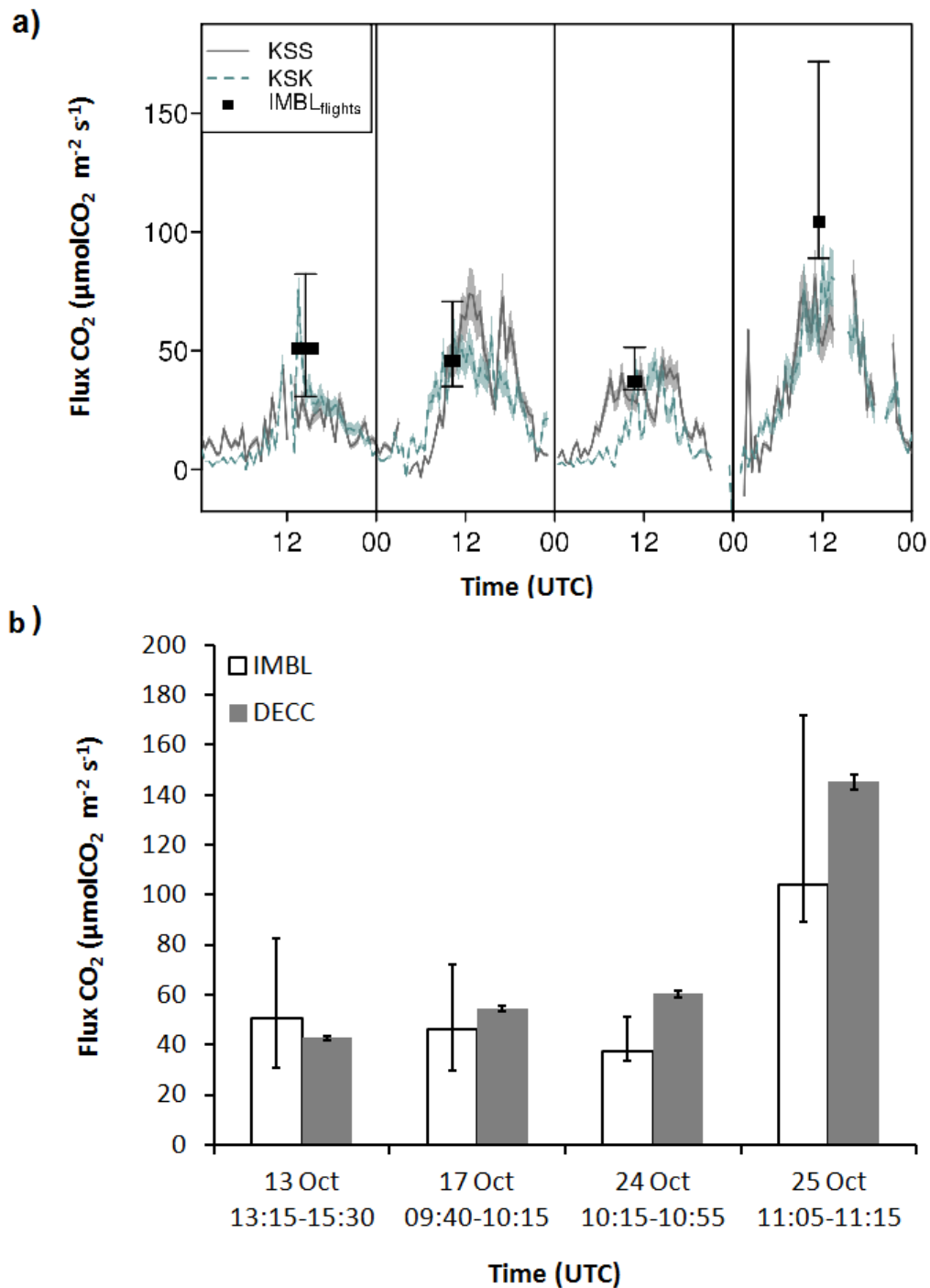
299 Our sensitivity analysis suggests that horizontal variability of the CO_2 field in the UBL, observed here
300 by transects, is the most critical factor affecting $F_{CO_2,IMBL}$. The determination of the BL height and vertical wind
301 speed has more impact on $F_{CO_2,IMBL}$ from upwind-downwind profiles.

302

303 3.2.4 CO_2 surface fluxes in Greater London

304 Aircraft-based $F_{CO_2,IMBL}$ and tower-based $F_{CO_2,EC}$ have complementary spatial and temporal resolutions
305 and limitations (Lloyd et al. 2007; Desai et al. 2011). With two EC systems in central London, the intra-site
306 variability in the $F_{CO_2,EC}$ could be assessed (Fig 4a). The lower KSK site (smaller source area) is expected to be
307 dominated by processes at the building-scale, while the taller KSS site is representative of the neighbourhood-
308 scale (Kotthaus and Grimmond, 2013b) and $F_{CO_2,IMBL}$ represent a larger area (10^2 - 10^4 km²) and integrate
309 processes at the city-scale.

310 Although direct comparison of $F_{CO_2,EC}$ and $F_{CO_2,IMBL}$ is not necessarily warranted given the lack of
311 immediate correspondence, Levy et al. (1999) argue that results should be within the same range and show
312 similar variation day-to-day. On 17 and 24 October, $F_{CO_2,EC}$ and $F_{CO_2,IMBL}$ have similar magnitude at the times
313 when IMBL were calculated (Figure 4a), while the $F_{CO_2,IMBL}$ is higher than the observed surface flux on 13
314 October and even more clearly so (by at least $20 \mu\text{mol CO}_2 \text{ m}^{-2} \text{ s}^{-1}$) on 25 October. These discrepancies may be
315 explained partly by the uncertainties inherent in the IMBL method (Table 3), but the EC measurements may also
316 underestimate the turbulent flux (as noted by Kotthaus and Grimmond 2013b). In terms of day-to-day variations,
317 the EC and IMBL method both indicate similarly strong fluxes on 13, 17 and 24 October and also agree in
318 estimating the largest fluxes on the 25 October.



320

321

322

323

324

325

326

Figure 4 (a) Time series of turbulent fluxes of CO_2 as observed at eddy covariance sites KSS and KSK in central London (lines) and estimates from the aircraft observations (rectangles). The EC errors are shaded assuming $\pm 15\%$ error on the 30 mins fluxes based on Euster et al. (1997), Dragoni et al. (2007) and Richardson et al. (2012) (b) Comparison of the surface fluxes calculated from aircraft observations (IMBL) against spatially integrated emissions as calculated from the DECC emissions inventory. Error bars on IMBL fluxes denote maximum and minimum values.

327 The annual CO₂ emissions for GL in 2011 were 18.3 μmolCO₂ m⁻² s⁻¹ (DECC, 2014). Scaling the
328 footprint area for temporal variations of the emissions, IMBL fluxes are within -37% (24 October) and 19% (13
329 October) of the DECC emissions. The differences between the $F_{CO_2,IMBL}$ and $F_{CO_2,inv}$ on 24 October may relate to
330 the $F_{CO_2,IMBL}$ footprint area encompassing large areas outside GL (Fig. 3e) and/or the uncertainty in the temporal
331 scaling.

332 Day-to-day differences in $F_{CO_2,IMBL}$ are partly attributed to variations in the flux source area given that
333 IMBL fluxes were calculated for similar times (except for 13 October). The DECC annual $F_{CO_2,inv}$ has a
334 concentric pattern: central GL boroughs have emissions of 50-350 μmol CO₂ m⁻² s⁻¹, surrounding centre
335 boroughs 25-50 μmol CO₂ m⁻² s⁻¹, and outer boroughs <25 μmol CO₂ m⁻² s⁻¹. The highest $F_{CO_2,IMBL}$ (October 25)
336 was found when the footprint area encompassed the high emission central boroughs. Although the 17 October
337 footprint also sampled central London, the calculated air residence times were shorter (10-30 s, Fig. 3c,d) (25
338 October, 70-140 s, Fig. 3f) and the probable footprint included the lower emission area of south-west GL. On 24
339 October the probable footprint extended over the outer boroughs to the west and south-west of GL (average
340 annual emissions <25 μmolCO₂ m⁻² s⁻¹).

341

342 **4 Discussion and conclusions**

343 Here we have presented four airborne surveys that measured CO₂ mixing ratios in the UBL of GL in
344 October 2011 that were used to estimate urban-scale emissions by quantifying boundary layer growth,
345 entrainment processes and horizontal transport. The top-down inverse IMBL method infers temporally and
346 spatially integrated fluxes that can be used to evaluate emissions inventories at policy-relevant scales such as
347 cities, megacities, and oil and gas fields. Previously, this approach has been used to infer nocturnal fluxes of
348 GHG with a single ground-level measurement site (Zimnoch et al. 2010), but inclusion of anthropogenic
349 emissions for critical daytime activities was missing. Entrainment and advection fluxes are usually not
350 considered in the calculations based on ground-level observations due to a lack of measurements at the top of
351 the BL and the spatial gradient of CO₂. However, as shown in this study, the entrainment term (13 October) and
352 advection (17 October) terms can be large fractions of the urban carbon budget. Observations from light aircraft
353 characterize different parts of the budget to permit calculation of integrated regional surface CO₂ fluxes at larger
354 scales than ground-level observations. Complementary aircraft surveys characterizing entrainment, vertical
355 mixing and spatial heterogeneity in the UBL add value to continuous measurements at ground-level (Strong et

356 al., 2011). However, aircraft observations are time-limited (e.g. plane time, flight path access) and weather-
357 biased, so represent case studies.

358 The IMBL fluxes had similar day-to-day variability to both the central London eddy-covariance
359 observations and the scaled (temporal, spatial) emissions inventory data. The IMBL fluxes are the same order as
360 the eddy-covariance observations and within -37% to 19% of the emissions inventory. Thus the IMBL method
361 appears to provide an additional independent estimate of city-scale fluxes to complement neighbourhood-scale
362 eddy-covariance fluxes and emissions inventory data.

363 The sensitivity tests undertaken suggest differences of the order of 100% in $F_{CO_2,IMBL}$ consistent with
364 other city-scale fluxes derived from aircraft measurements using mass-balance approaches (e.g. for GHG Mays
365 et al. 2009; Turnbull et al. 2011, NO_x emissions Trainer et al. 1995). However, changes in UBL CO₂
366 concentration along large city transects may challenge city-wide emission quantification as this was the main
367 source of uncertainty for IMBL fluxes. Atmospheric transport and surface exchange are continuous, creating a
368 dynamic, complex picture in large cities that can hardly be resolved in short-term airborne campaigns (Gioli et
369 al. 2014). This suggests that in a megacity such as London it may be necessary to consider internal boundary
370 layers (IBL) within the city. The atmosphere above the outer boroughs, which are more extensive and typically
371 have shorter roughness elements (e.g. buildings), may be well mixed, but over the central business district areas
372 where the buildings are much taller the BL at the flight height may be the IBL for that area rather than the fully
373 mixed UBL. Thus more detailed knowledge of the BL dynamics over urban areas is critical. Moreover, the rate
374 of emission along a transect may temporally vary producing spatial variations of CO₂ within the UBL.

375 Downwind [CO₂] enhancements above the background concentration are more representative of the
376 mix of emissions taking place in the urban environment. A single pair of upwind-downwind profiles does not
377 sample the entire urban area (Fig. 3e,f). In order to overcome this, multiple downwind profiles should be
378 sampled in future surveys.

379 Footprint analysis allows identification of the areas potentially contributing to CO₂ concentrations in
380 the UBL. Emissions from the inventory have been scaled for the footprint of airborne measurements and it
381 might be a source of uncertainty. For better comparison of emissions and IMBL fluxes, meso-scale modelling
382 such as the proposed by Brioude et al. (2013) could enhance better spatial scaling of the fluxes.

383 Anthropogenic and biogenic fluxes are inherently included in $F_{CO_2,EC}$ and $F_{CO_2,IMBL}$, whereas biogenic
384 fluxes are missing from the $F_{CO_2,inv}$ fluxes. The role of vegetation varies with amount (e.g. Helfter et al. 2011),
385 but generally in urban areas it plays a small role in the CO₂ budget (Crawford et al. 2011, Strong et al. 2011;

386 Newman et al. 2013). In London the vegetation varies by size (age) and type across the city (Lindberg and
387 Grimmond 2011). By October the role of vegetation is likely small during the daytime relative to urban sources
388 even in suburban areas with a large amount of vegetation (Ward et al. 2013). To distinguish the anthropogenic
389 signal, fast-response measurements of urban pollutants (e.g. NO_x, CO) as tracers of traffic-related emission and
390 isotopic analysis of carbon (e.g. ¹³C/¹²C-CO₂, Δ¹⁴CO₂) would aid interpretation. An emissions ratio approach
391 (e.g. Turnbull et al. 2011) would allow apportionment and identification of the sectors emitting more CO₂ into
392 the atmosphere and thus facilitate evaluation of policy effectiveness to reduce the contribution of GHG
393 emissions from urban areas.

394

395 **Acknowledgements**

396 The flights were undertaken as part of the ClearfLo project funded by the Natural Environment
397 Research Council (NERC) and coordinated by the National Centre for Atmospheric Science (NCAS). The
398 flights surveys were supported by the NERC-ARSF grant (GB11-05). We would like to thank the crew and the
399 operations team of the ARSF team. We extend our thanks to Rebecca Fisher at Royal Holloway University of
400 London (RHUL) for the calibration to the NOAA standards of the references used for the surface monitoring
401 sites. We are grateful to the Lab of the Atmosphere and the Oceans from the Institut Català de Ciències del
402 Clima (LAO-IC3) for the airborne CO₂ instrument and in-flight standards and the insightful comments of
403 reviewers which improved the paper. The research was supported by the National Institute for Health Research
404 (NIHR) Biomedical Research Centre based at Guy's and St Thomas' NHS Foundation Trust and King's College
405 London and NERC ClearfLo (NE/H003231/1).

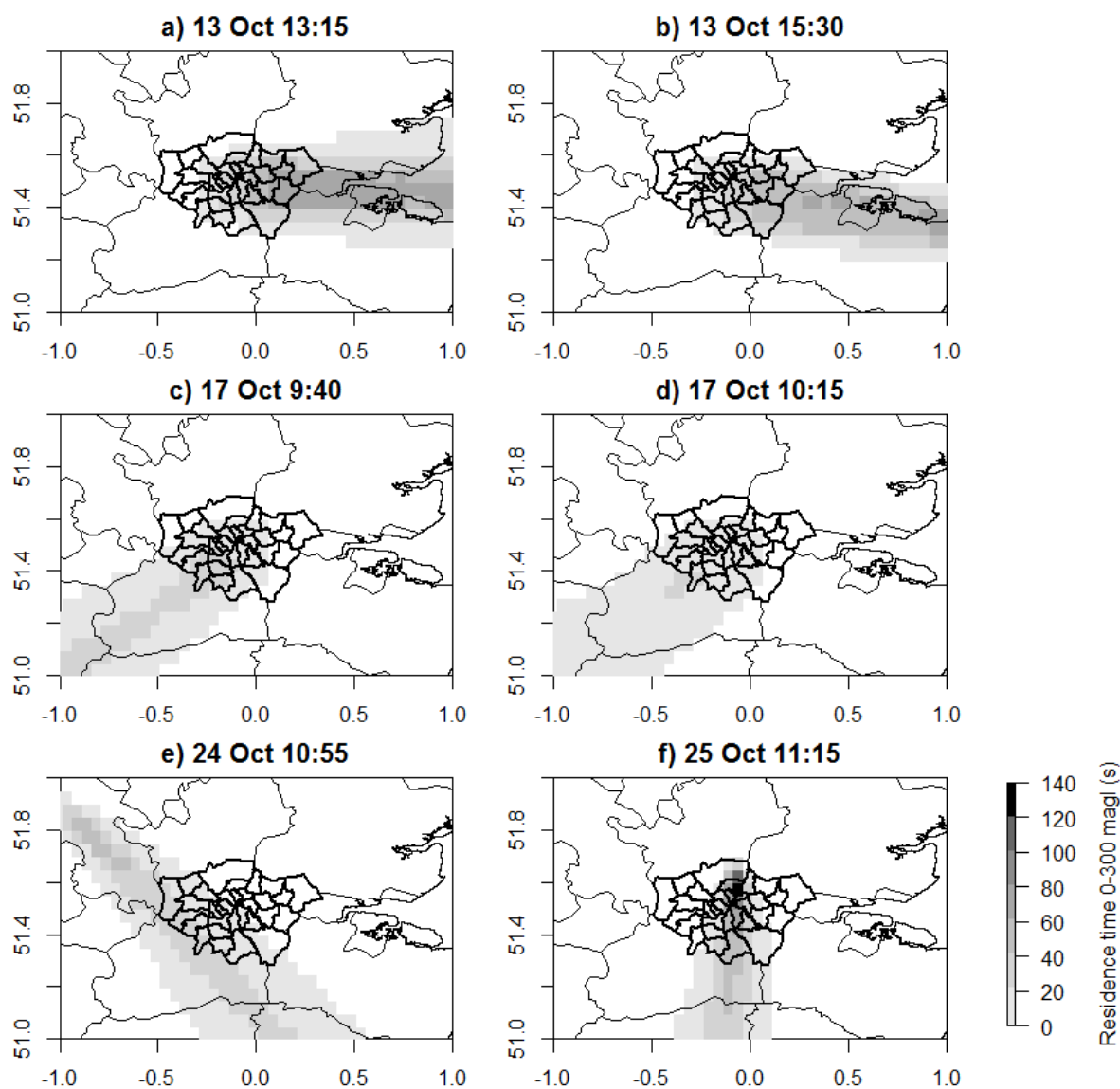
406 **Figures**

407 Fig. 1: B&W (print version)

408 Fig. 2: B&W (print version)

409 Fig. 3: B&W (print version), Colour (web version)

410 Fig. 4: B&W (print and web version)



411

412

Figure 3 in B&W for print version

413 **References**

414 Beswick, K.M., Gallagher, M.W., Webb, A.R., Norton, E.G. & Perry, F. (2008). Application of the
 415 Aventech AIMMS20AQ airborne probe for turbulence measurements during the Convective Storm Initiation
 416 Project. *Atmospheric Chemistry and Physics*, 8, 5449–5463.

417 Brioude, J., Angevine, W.M., Ahmadov, R., Kim, S.-W., Evan, S., McKeen, S.A., Hsie, E.-Y.,
 418 Frost, G. J., Neuman, J.A., Pollack, I.B., Peischl, J., Ryerson, T.B., Holloway, J., Brown, S.S., Nowak, J.B.,
 419 Roberts, J.M., Wofsy, S.C., Santoni, G.W., Oda, T., Trainer, M. (2013). Top-down estimate of surface flux in
 420 the Los Angeles Basin using a mesoscale inverse modeling technique: assessing anthropogenic emissions of

421 CO, NO_x and CO₂ and their impacts, *Atmospheric Chemistry and Physics*, 13, 3661-3677, doi:10.5194/acp-13-
422 3661-2013.

423 Christen, A. (2014). Progress in atmospheric measurement techniques to quantify greenhouse gas
424 emissions from cities, *Urban Climate*, in press, doi: 10.1016/j.uclim.2014.04.006

425 Cleugh H.A., Grimmond, C.S.B. (2001). Modeling regional scale surface energy exchanges and CBL
426 growth in a heterogeneous, urban-rural landscape. *Boundary Layer Meteorology*, 98, 1-31.

427 Crawford, B., Grimmond, C.S.B. & Christen, A. (2011). Five years of carbon dioxide fluxes
428 measurements in a highly vegetated suburban area. *Atmospheric Environment*, 45, 1564–1573.

429 Denmead, O.T., Raupach, M.R., Dunin, F.X., Cleugh, H.A., Leuning, R. (1996). Boundary-Layer
430 Budgets for Regional Estimates of Scalar Fluxes. *Global Change Biology*, 2, 255–264.

431 Department of Energy and Climate Change (DECC) (2014):
432 <https://www.gov.uk/government/statistics/local-authority-emissions-estimates> (last access: 28 August 2014).

433 Desai, A.R., Moore, D.J.P., Ahue, W.K.M., Wilkes, P.T.V., De Wekker, S.F.J., Brooks, B.G., Campos,
434 T.L., Stephens, B.B., Monson, R.K., Burns, S.P., Quaife, T., Aulenbach, S.M., Schimel, D.S. (2011). Seasonal
435 pattern of regional carbon balance in the central Rocky Mountains from surface and airborne measurements,
436 *Journal Geophysical Research*, 116, G04009, doi:10.1029/2011JG001655.

437 Dragoni D., Schmid, H.P., Grimmond, C.S.B., Loescher, H.W. (2007) Uncertainty of annual net
438 ecosystem productivity estimated using eddy covariance flux measurements, *Journal Geophysical Research*,
439 112, D17102.

440 Duren, R.M., Miller, C.E. (2012). Measuring the carbon emissions of megacities. *Nature Climate
441 Change*, 2, 560-562.

442 Eugster, W., McFadden, J.P., Chapin, E.S. (1997). A comparative approach to regional variation in
443 surface fluxes using mobile eddy correlation towers, *Boundary Layer Meteorology*, 85, 293–307.

444 Feigenwinter, C., Vogt, R., Christen, A. (2012). Eddy Covariance Measurements Over Urban Areas in
445 Eddy Covariance, *Springer Atmospheric Sciences*, 377-397.

446 Font, A., Morguá, J.-A., Rodó, X. (2008). Atmospheric CO₂ in-situ measurements: two examples of
447 Crown Design flights in NE Spain. *Journal of Geophysical Research*, 113, D12308,
448 doi:10.1029/2007JD009111.

449 Font, A., Morguá, J.-A., Curcoll, R., Pouchet, I., Casals, I., Rodó, X. (2010). Daily carbon surface fluxes
450 in the West Ebre (Ebro) watershed from aircraft profiling on late June 2007. *Tellus*, 62B, 427-440.

451 Gioli, B., Carfora, M. F., Magliulo, V., Metallo, M.C., Poli, A.A., Toscano, P., Miglietta, F. (2014).
452 Aircraft mass budgeting to measure CO₂ emissions of Rome, Italy. *Environmental Monitoring and Assessment*,
453 186, 2053–2066, doi: 10.1007/s10661-013-3517-4.

454 Grimmond, C.S.B., King, T.S., Cropley, F.D., Nowak, D.J., Souch, C. (2002). Local-scale fluxes of
455 carbon dioxide in urban environments: methodological challenges and results from Chicago. *Environmental*
456 *Pollution*, 116, S243-S254.

457 Guenther, A., Zimmerman, P., Klinger, L., Greenberg, J., Ennis, C., Davis, K. & Pollock, W. (1996).
458 Estimates of regional natural volatile organic compound fluxes from enclosure and ambient measurements.
459 *Journal of Geophysical Research*, 101, D1, 1345-1359.

460 Helfter, C., Famulari, D., Phillips, G. J., Barlow, J. F., Wood, C. R., Grimmond, C.S.B., Nemitz, E.
461 (2011), Controls of carbon dioxide concentrations and fluxes above central London, *Atmospheric Chemistry and*
462 *Physics*, 11, 1913–1928, doi:10.5194/acp-11-1913-2011.

463 International Energy Agency (IEA) (2008). World Energy Outlook, 2008, Paris, France

464 Idso, C.D., Idso, S.B. & Balling, R.C., Jr. (1998). The urban CO₂ dome of Phoenix, Arizona. *Physical*
465 *Geography*, 19, 95-108.

466 Jacob, D.J. (1999). Introduction to Atmospheric Chemistry. *Princeton University Press*, 267 pp.

467 Kordowski, K., Kuttler, W. (2010). Carbon dioxide fluxes over an urban park area. *Atmospheric*
468 *Environment*, 44, 2722-2730.

469 Kormann, R., Meixner, F. X. (2001). An Analytical Footprint Model for Non-Neutral Stratification.
470 *Boundary Layer Meteorology*, 99, 207–224.

471 Kotthaus, S., Grimmond, C.S.B. (2012). Identification of Micro-scale Anthropogenic CO₂, Heat and
472 Moisture Sources – Processing Eddy Covariance Fluxes for a Dense Urban Environment. *Atmospheric*
473 *Environment*, 57, 301-316, doi: 10.1016/j.atmosenv.2012.04.024.

474 Kotthaus, S., Grimmond, C.S.B. (2013a). Energy exchange in a dense urban environment – Part I:
475 temporal variability of long-term observations in central London, *Urban Climate*, in press.

476 Kotthaus, S., Grimmond, C.S.B. (2013b). Energy exchange in a dense urban environment – Part II:
477 impact of spatial heterogeneity of the surface, *Urban Climate*, in press.

478 Levy, P.E., Grelle, A., Lindroth, A., Mölder, M., Jarvis, P.G., Kruijt, B., Moncrieff, J.B. (1999).
479 Regional-scale CO₂ fluxes over central Sweden by a boundary layer budget method. *Agricultural and Forest*
480 *Meteorology*, 98–99, 169–180.

481 Lindberg, F, Grimmond, C.S.B. (2011) Nature of vegetation and building morphology characteristics
482 across a city: influence on shadow patterns and mean radiant temperatures in London, *Urban Ecosystems*, 14(4),
483 617-634, doi: 10.1007/s11252-011-0184-5

484 Lloyd, J., Francey, R J., Mollicone, D., Raupach, M.R., Sogachev, A., Arneth, A., Byers, J.N., Kelliher,
485 F.M., Rebmann, C., Valentini, R., Wong, S.-C., Bauer, G., Schulze, E.-D. (2001). Vertical profiles, boundary
486 layer budgets, and regional flux estimates for CO₂ and its ¹³C/¹²C ratio and for water vapor above a forest/bog
487 mosaic in central Siberia. *Global Biogeochemical Cycles*, 15(2), 267–284, doi:10.1029/1999GB001211.

488 Lloyd, J., Kolle, O., Fritsch, H., De Freitas, S.R., Silva Dias, M.A.F., Artaxo, P., Nobre, A.D., De
489 Araújo, A.C., Kruijt, B., Sogacheva, L., Fisch, G., Thielmann, A., Kuhn, U., Andreae, M.O. (2007). An
490 airborne regional carbon balance for Central Amazonia. *Biogeosciences*, 4, 759-768.

491 MacCarthy (2014). Local and Regional Carbon Dioxide Emissions Estimates for 2005-2012 for the UK
492 Technical Report, available at
493 [https://www.gov.uk/government/uploads/system/uploads/attachment_data/file/322833/20120624_Local_CO2_-](https://www.gov.uk/government/uploads/system/uploads/attachment_data/file/322833/20120624_Local_CO2_-_Technical_Report_2012.pdf)
494 [_Technical_Report_2012.pdf](https://www.gov.uk/government/uploads/system/uploads/attachment_data/file/322833/20120624_Local_CO2_-_Technical_Report_2012.pdf) (last access: 28August 2014).

495 Mays, K.L., Shepson, P.B., Stirm, B.H., Karion, A., Sweeney, C., Gurney K.R. (2009). Aircraft-Based
496 Measurements of the Carbon Footprint of Indianapolis. *Environment Science Technology*, 43, 7816–7823.

497 McNaughton, K.G., Spriggs, T.W. (1986). A Mixed-Layer Model for Regional Evaporation. *Boundary-*
498 *Layer Meteorology*, 34, 243–263.

499 Nemitz, E., Hargreaves, K.J., McDonald, A.G., Dorsey, J.R., Fowler, D. (2002). Micrometeorological
500 measurements of the urban heat budget and CO₂ emissions on a city scale. *Environmental Science and*
501 *Technology*, 36(14), 3139-3146.

502 Newman, S., Jeong, S., Fischer, M. L., Xu, X., Haman, C. L., Lefer, B., Alvarez, S., Rappenglueck, B.,
503 Kort, E. A., Andrews, A. E., Peischl, J., Gurney, K. R., Miller, C. E., Yung, Y. L. (2013). Diurnal tracking of
504 anthropogenic CO₂ emissions in the Los Angeles basin megacity during spring 2010, *Atmos. Chem. Phys.*, 13,
505 4359-4372, doi:10.5194/acp-13-4359-2013.

506 Pataki, D.E., Bowling, D.R., Ehleringer, J.R., Zobitz, J.M. (2006). High resolution atmospheric
507 monitoring of urban carbon dioxide sources. *Geophysical Research Letters*, 33, L03813,
508 doi:10.1029/2005GL024822.

509 Raupach, M.R. (1992). Drag and Drag Partition on Rough Surfaces. *Boundary-Layer Meteorology*, 60,
510 375–395.

542 Richardson, A. D., Aubinet, M., Barr, A. G., Hollinger, D. Y., Ibrom, A., Lasslop, G., Reichstein, M.
543 (2012). Uncertainty Quantification in M. Aubinet et al. (eds.), *Eddy Covariance: A Practical Guide to*
544 *Measurement and Data Analysis*, Springer Atmospheric Sciences, Springer Science C Business Media B.V.

545 Schmid, H.P. (1994). Source Areas for Scalars and Scalar Fluxes. *Boundary Layer Meteorology*, 67,
546 293–318.

547 Spanton, A.M. & Williams, M.L. (1988). A comparison of the structure of the atmospheric boundary
548 layers in central London and a rural suburban site using acoustic sounding. *Atmospheric Environment*, 22 (2),
549 211–223.

550 Stohl, A., Forster, C., Frank, A., Seibert, P., Wotawa, G. (2005). Technical note: the Lagrangian particles
551 dispersion model FLEXPART version 6.2. *Atmospheric Chemistry and Physics*, 5, 2461–2474.

552 Strong, C., Stwertka, C., Bowling, D.R., Stephens, B.B., Ehleringer, J.R. (2011), Urban carbon dioxide
553 cycles within the Salt Lake Valley: A multiple-box model validated by observations, *Journal Geophysical*
554 *Research*, 116, D15307, doi:10.1029/2011JD015693.

555 Stull, R. B. (1988). *An Introduction to Boundary Layer Meteorology*, Springer, New York.

556 Trainer, M., Ridley, B.A., Buhr, M.P, Kok, G., Walega, J., Hiibler, G., Parrish, D. D., Fehsenfeld, F.
557 C. (1995), Regional ozone and urban plumes in the southeastern United States: Birmingham, a case study,
558 *Journal Geophysical Research*, 100, D9, 18823-18834.

559 Turnbull, J.C., Karion, A., Fischer, M.L., Faloona, I., Guilderson T., Lehman, S J., Miller, B.R., Miller,
560 J.B., Montzka, S., Sherwood T., Saripalli, S., Sweeney C. & Tans, P.P. (2011). Assessment of fossil fuel carbon
561 dioxide and other anthropogenic trace gas emissions from airborne measurements over Sacramento, California
562 in spring 2009. *Atmospheric Chemistry and Physics*, 11, 705–721, doi:10.5194/acp-11-705-2011.

563 Velasco, E., Roth, M. (2010). Cities as net sources of CO₂: review of atmospheric CO₂ exchange in urban
564 environments measured by Eddy Covariance technique. *Geography Compass*, 4, 1238–1259, doi:
565 10.1111/j.1749-8198.2010.00384.x.

566 Ward, H. C., Evans, J.G., Grimmond, C.S.B. (2013). Multi-season eddy covariance observations of
567 energy, water and carbon fluxes over a suburban area in Swindon, UK. *Atmospheric Chemistry and Physics*, 13,
568 4645–4666.

569 Zimnoch, M., Godłowska, J., Necki, J.M., Rozanski, K. (2010). Assessing surface fluxes of CO₂ and CH₄
570 in urban environment: a reconnaissance study in Krakow, Southern Poland. *TellusB*, 62, 573–580, doi:
571 10.1111/j.1600-0889.2010.00489.x.